ACS APPLIED MATERIALS & INTERFACES

www.acsami.org

Research Article

One-Step Generation of Aqueous-Droplet-Filled Hydrogel Fibers as Organoid Carriers Using an All-in-Water Microfluidic System

Hui Wang,[&] Haitao Liu,[&] Xu Zhang,[&] Yaqing Wang, Mengqian Zhao, Wenwen Chen, and Jianhua Qin*

Cite This: https://dx.doi.org/10.1021/acsami.0c20434

Read Online

ACCESS | Metrics & More | Article Recommendations | Supporting Information

ABSTRACT: Hydrogel fibers are promising carriers for biological applications due to their flexible mechanical properties, well-defined spatial distribution, and excellent biocompatibility. In particular, the droplet-filled hydrogel fibers with the controllable dimension and location of droplets display great advantages to enhance the loading capacity of multiple components and biofunctions. In this work, we proposed a new all-in-water microfluidic system that allows for one-step fabrication of aqueous-droplet-filled hydrogel fibers (ADHFs) with unique morphology and tunable configurations. In the system, the aqueous droplets with equidistance are successfully arranged within the alginate calcium fibers, relying on the design of the pump valve cycle and the select of two immiscible liquids with a stable aqueous interface. The architecture of the ADHF can be flexibly controlled by adjusting the three phase flow rates and the valve switch cycle. The produced ADHFs exhibit high controllability, uniformity, biocompatibility, and stability. The established system enabled the formation of functional human islet organoids in situ through encapsulating pancreatic endocrine progenitor cells within microfibers. The generated islet organoids within droplets exhibit high cell viability and islet-specific function of insulin secretion. The proposed approach provides a new way to fabricate multifunctional hydrogel fibers for materials sciences, tissue engineering, and regenerative medicine.

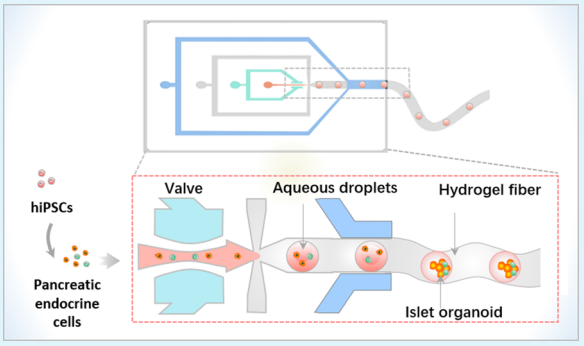

KEYWORDS: *all-in-water microfluidic system, aqueous-droplet-filled hydrogel fiber (ADHF), one-step fabrication, islet organoids, tissue engineering*

INTRODUCTION

Hydrogel fibers have emerged as promising scaffolds in materials science, cell biology, and tissue engineering for their large specific surface area, excellent biodegradability, and flexible mechanical properties.[1−7] Hydrogel fibers are widely used in transplant carriers,[8,9] drug delivery,[10] and hydrogel sensors,[11,12] which are produced by coating,[13] electrospinning,[14,15] bioprinting,[16−18] and microfluidics.[19] In recent years, the microfluidic technique has been utilized as a versatile tool to fabricate the hydrogel fibers with various structures, compositions, and functions due to the flexibility of chip design and the accuracy of flow control.[20] Generally, a stable liquid jet is surrounded by a sheath flow during the process of microfluidic spinning. Then, solid fibers are produced via a physical and/or chemical reaction.[21] According to morphological characteristics, the hydrogel fibers generated via microfluidic technology can be generally categorized into tubular,[22,23] grooved,[24,25] helical,[26−28] and knotted fibers.[29] Among them, the knotted hydrogel fibers, or called droplet-filled hydrogel fibers (DHFs) with tunable size and space of droplets, display great advantages to enhance the loading capacity with multiple components and to promote the formation of cell clusters with multi-functions.

Recently, numerous works with consecutive emulsification steps have been reported to produce oil-encapsulated hydrogel fibers using an oil−water microfluidic system based on the stability of the interface between oil and water phases.[30−35] These reports overcome the challenge of the structural simplicity of DHFs fabricated in traditional ways and promote the development of loading the hydrophobic substance in oil droplets of the hydrogel fiber. However, these methods are limited by the existing of oil phase in the fibers, which would affect the viability and functions of the encapsulated cells or tissues. Also, the oil phase of the droplet may block the molecular exchange in the fiber.[36−38] One group has taken the effort to produce both aqueous-droplet- and oil-droplet-filled hydrogel fibers with the help of an aqueous two-phase system (ATPS).[38] Nevertheless, the oil phase is unavoidably introduced as a chopper into such a fiber that is not an ideal

Received: November 16, 2020
Accepted: December 22, 2020

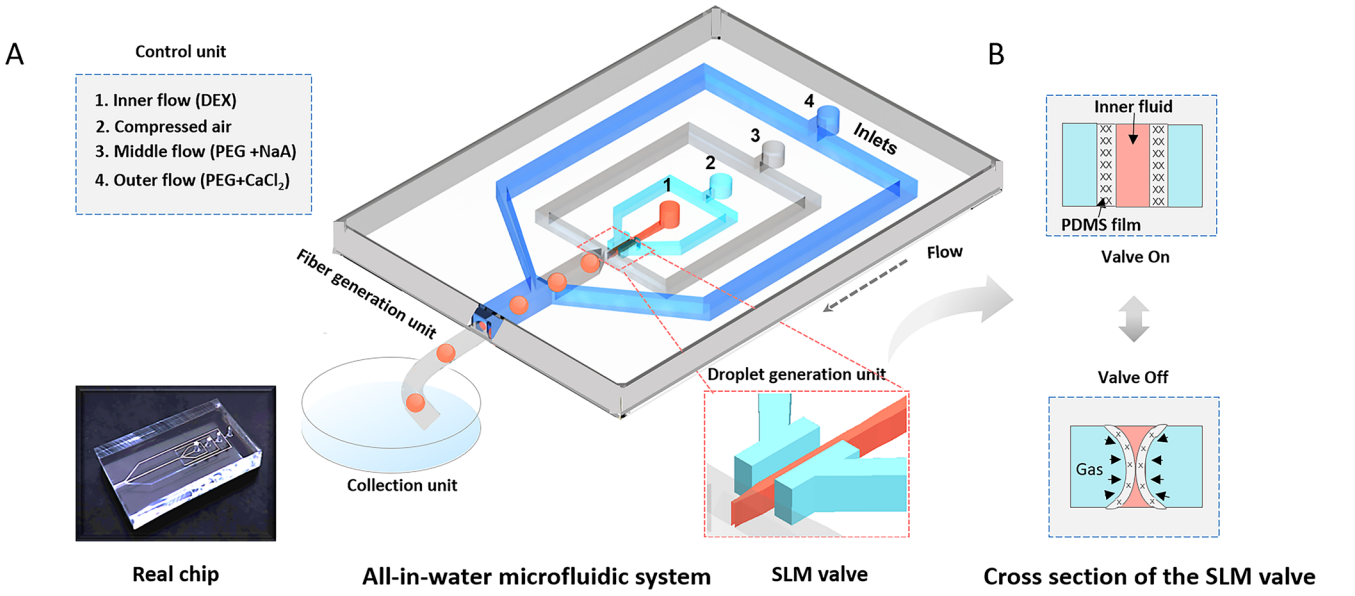

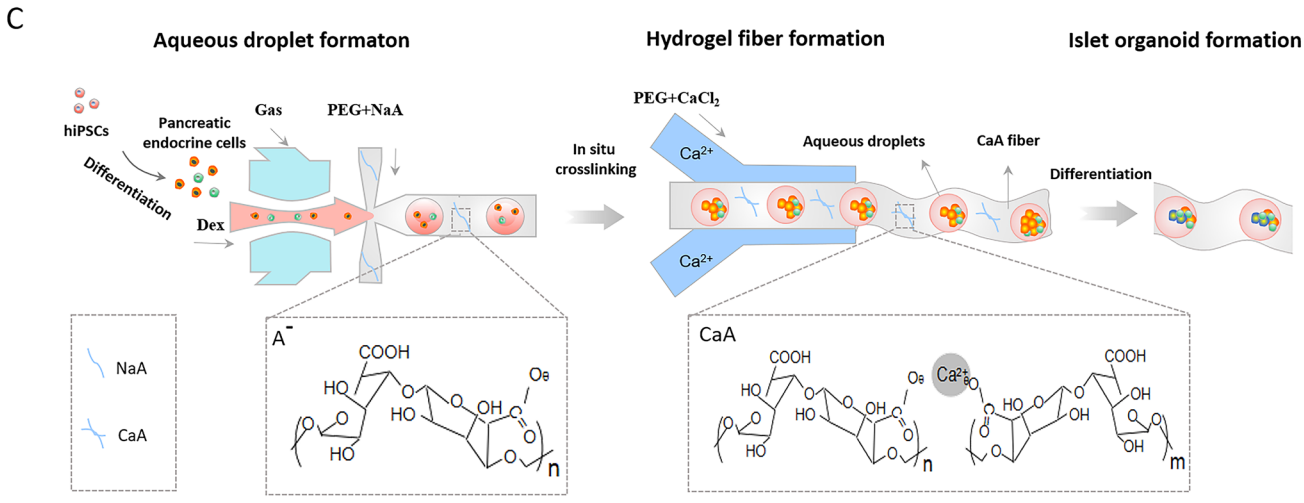

Synthetic principle of the aqueous-droplet-filled hydrogel fibers (ADHF) as organoids carriers

Figure 1. Schematic diagram of the all-in-water microfluidic system to generate aqueous-droplet-filled hydrogel fiber (ADHF) that enables 3D culture of islet organoids. (A) Configuration of the microfluidic chip containing fluid inlets/outlet units, aqueous droplet generation unit, fiber generation unit, and collection unit. (B) Cross section of the SLM (single-layer membrane) valve. (C) Procedures for generation of ADHF serving as carriers for engineering islet organoids derived from human induced pluripotent stem cell (hiPSC).

carrier for biomedical applications. Therefore, the flexible generation of ADHF with high biocompatibility and good functionality is still a huge challenge. To overcome these challenges, the generation of ADHF within an oil-free system is needed. All-in-water microfluidic systems provide a unique oil-free art to meet this demand.[39,40] To our knowledge, the generation of ADHF using an all-in-water microfluidic system has never been reported before.

Here, we provided a novel methodology to generate ADHF with aqueous droplets arrayed in calcium alginate (CaA) fibers based on an all-in-water microfluidic system. A pneumatic valve is designed in the flow-focusing microfluidic chip to facilitate the production of ADHF, enhance the controllability, and improve the operability. Stable aqueous droplets are created using the auxiliary pump that separate the active phases of the dextran (Dex) and poly(ethylene glycol) (PEG) in the inner and middle flows followed by the fast reaction of ion cross-linking between the sodium alginate (NaA) and calcium chloride ($CaCl_2$) within middle and outer fluids. The morphology of the ADHF, such as the size and interval of droplets, can be flexibly controlled by tuning the three phase flow rates and the valve switch cycle. To demonstrate the possibility of the ADHF as bio-carriers for the 3D culture of organoids, pancreatic endocrine progenitor cells from human induced pluripotent stem cells (hiPSCs) are encapsulated in the droplets of fibers. The generated islet organoids exhibit good cell viability and high expression of islet-specific genes and sensitive glucose-stimulated insulin secretion (GSIS). The proposed all-in-water microfluidic approach is controllable and flexible, paving a new way to fabricate multifunctional bio-fibers for micro-tissues and organoid engineering.

https://dx.doi.org/10.1021/acsami.0c20434
ACS Appl. Mater. Interfaces XXXX, XXX, XXX−XXX

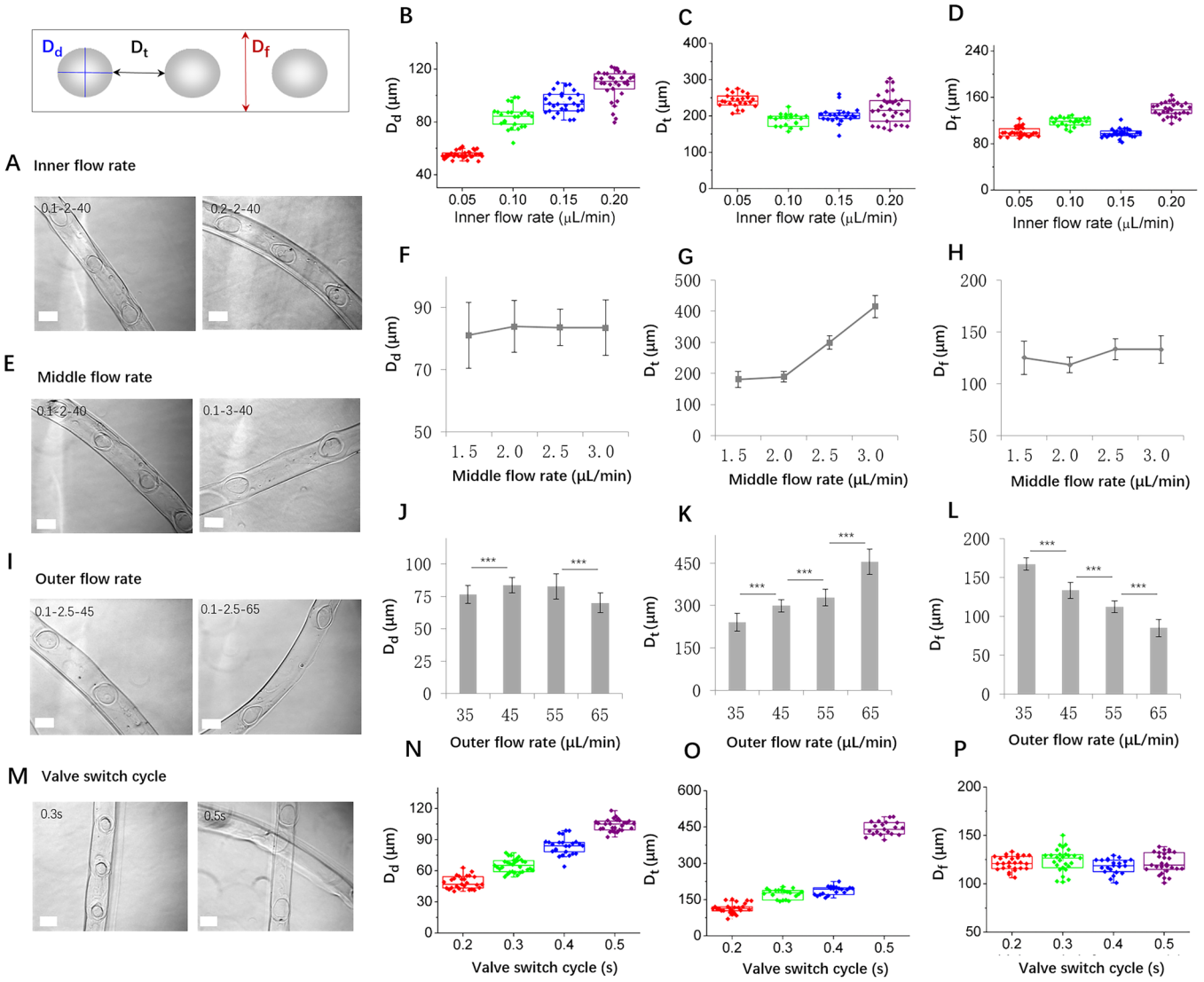

Figure 2. Effects of three-phase fluids and the valve switch cycle on the droplet diameter (D_d), droplet distance (D_t), and fiber diameter (D_f). (A) Bright-field images of ADHF fabricated under variable rates of inner-phase flow (0.1 and 0.2 μL/min). (B−D) Effects of the inner-phase flow rate on D_d, D_t, and D_f from 0.05 to 0.20 μL/min. The middle-phase and the outer-flow rates were fixed to 2 and 40 μL/min, respectively. (E) Bright-field images of ADHF generated under variable rates of middle-phase flow (2 and 3 μL/min). (F−H) Effects of the middle-phase flow rate on D_d, D_t, and D_f from 1.5 to 3.0 μL/min. The inner-phase and the outer-flow rates were fixed to 0.1 and 40 μL/min, respectively. (I) Bright-field images of ADHF generated under variable rates of outer-phase flow (45 and 65 μL/min). (J−L) Effects of the outer-phase flow rate on D_d, D_t, and D_f from 35 to 65 μL/min. The inner-phase and the middle-flow rates were fixed to 0.1 and 2.5 μL/min, respectively. (M) Bright-field images of ADHF generated under variable valve switch cycles (0.3 and 0.5 s). (N−P) The effects of valve switch cycles on D_d, D_t, and D_f from 0.2 to 0.5 s. The inner-phase, middle-phase, and the outer-flow rates were fixed to 0.1, 2, and 40 μL/min, respectively. *p < 0.05 and ***p < 0.001. Scale bars: 100 μm.

RESULTS AND DISCUSSION

In order to generate ADHF in a controllable and flexible way, we designed and established a novel all-in-water microfluidic system. The proposed system combined the droplet microfluidic technology with the wet-spinning approach. As shown in Figure 1, the microfluidic device comprises a series of key units, including the fluid inlets/outlet unit, aqueous droplet generation unit, fiber generation unit, and collection unit (Figure 1A). In the system, the aqueous two-phase solutions containing Dex and PEG served as templates for the generation of ADHF. Specifically, 15% (w/w) Dex solution, 17% PEG solution containing 1% (w/w) NaA, and 17% (w/w) PEG solution containing 4% (w/w) $CaCl_2$ were introduced through an inner-phase inlet, middle-phase inlet, and outer-phase inlet, respectively. Since PEG is more hydrophobic than Dex,[41] the PEG in the middle phase has a better affinity with the PDMS channel, which leads to a better coating effect during cell encapsulation. The key units of the device, including the aqueous droplet generation unit and fiber generation unit, are shown in Figure 1C. The "+" junction geometry of the aqueous droplet generation unit was used to form shear force between two immiscible liquids (Dex and PEG) for the generation of aqueous droplets. Meanwhile, pneumatic solenoid valves located beside the inner-phase channel were integrated in the aqueous droplet generation unit, which was utilized to improve the operability of the aqueous droplet generation and increase the stability and controllability of arranging the droplets into the ADHF. The cross section of the SLM valve and the schematic diagram are shown in Figure 1B. The pneumatic valve facilitated the

https://dx.doi.org/10.1021/acsami.0c20434
ACS Appl. Mater. Interfaces XXXX, XXX, XXX−XXX

generation of aqueous droplets, enhanced the controllability, and improved the operability (Figure S1). This enables the generation of an ADHF containing pre-defined aqueous droplet arrays. In addition, compared to the traditional hydrogel spheres, the ADHF shows superior advantages in terms of the functions and potential applications. The ADHF can be served as uniform carriers with multiple compartments, which can be used to carry a variety of chemical components or cell spheroids and can be easily assembled into higher-ordered structures.[23] These fibers can be used for the reconstruction of functional tissues with a fiber-shaped matrix, which can mimic the muscle tissue, blood vessels, or nerve networks.[23] Also, in the respect of potential diabetes treatment, the ADHF can be scaled up in the longitudinal direction to a large capacity, which enables easy handling, implantation, and retrieval. This property can minimize the safety risks of transplant and can be rapidly retrieved.[9]

A spinning nozzle was designed at the outlet of the channel for the fiber fabrication. Meanwhile, a traditional flow-focusing structure was designed to manipulate the laminar flow of the middle-phase and outer-phase fluids, which can avoid the clogging of the microchannel induced by the reaction between Ca^{2+} and NaA. Finally, CaA hydrogel fibers with good mechanical strength were formed in channels. The collection unit containing a 17% PEG solution was served to collect the ADHF. Under the supporting effect of the outer fiber, a delicate knotted structure can be realized. Here, the ADHF could serve as carriers for engineering islet organoids derived from human induced pluripotent stem cell (hiPSC). The synthetic principle is shown in Figure 1C. The aqueous droplets loaded in hydrogel fibers could improve the advantage of this approach in cell biological applications because of all the water environment and fiber structure. The ADHF well avoids the influence of the oil phase in the water−oil system, which would be favorable as cell carriers. The practicability of this ADHF is characterized by its capability to serve as a versatile carrier for controllably loading specific cells with different biomolecules and encoded materials.

To investigate the key factors of the all-in-water microfluidic system to fabricate monodispersed ADHF, we studied the diameter of droplets (D_d), the distance of droplets (D_t), and the diameter of fiber (D_f) under different conditions. Two major factors including the flow rates of multi-phase fluids and valve switch cycle were studied systematically. The valve switch cycle refers to the total time of the valve from being switched on to off, where the period of the valves switched on and off is equal in the experiment.

The flow rates of inner, middle, and outer phases were the main parameters in the system. To investigate the effects of flow rates on the formation of ADHF containing aqueous droplets, 15% (w/w) Dex, 17% (w/w) PEG + 1% (w/w) NaA, and 17% (w/w) PEG + 4% (w/w) $CaCl_2$ were injected as the inner, middle, and outer flows, respectively. Herein, the valve switch cycle was kept to 0.4 s.

First, we observed the effects of the inner phase on the generation of the ADHF with aqueous droplets. The middle phase and the outer flow rates were fixed to 2 and 40 μL/min, respectively. As shown in Figure 2A and Figure 2B−D, the flow rate of the inner phase affected the D_d from 55.25 ± 2.70 to 108.40 ± 11.04 μm (***$p < 0.001$) but did not influence the D_t and D_f ($p > 0.05$) when the flow rate of the inner phase was increased from 0.05 to 0.2 μL/min. Similarly, to evaluate the effects of middle phase, the flow rates of the inner phase and outer phase were then fixed to 0.1 and 40 μL/min, respectively. The flow rate of the middle phase was adjusted from 1.5 to 3.0 μL/min. As shown in Figure 2E and Figure 2F−H, D_t increased significantly with a rising middle phase flow rate from 187.40 ± 30.42 to 414.64 ± 35.52 μm (***$p < 0.001$), while no significant changes on D_d and D_f were observed ($p > 0.05$). These results revealed that the increasing flow rate of the middle phase only affected the spinning speed. The effect of the outer phase flow rate is shown in Figure 2I and Figure 2J−L. The increased outer phase flow rate (from 35 to 65 μL/min) affected D_t that varied from 241.52 ± 31.98 to 454.31 ± 44.99 μm (***$p < 0.001$), and D_f changed from 167.19 ± 8.02 to 84.89 ± 11.47 μm (***$p < 0.001$), which generated longer and thinner fibers under the same inner and middle flow rates. In the system, the coefficient of variation (CV, i.e., polydispersity) of the aqueous droplets ranged from 4.89 to 10.19% (Figure S2), indicating the good monodispersity of the aqueous droplets in fibers. Herein, the interfacial surface tension between two aqueous flows on the boundary is too low to maintain the spherical form,[42] which results in the distortion on the boundary of fibers at some droplet locations.

These results reflected that the size of droplets primarily relied on the flow rate of the inner phase, while the distance of aqueous droplets mainly depended on the flow rate of the middle phase and outer phase. The size of fiber mainly lied on the flow rate of the outer phase. Therefore, by flexibly changing the flow rates, the dimension of the ADHF and the location/size of the droplets could be flexibly controlled. Unlike oil-encapsulated hydrogel fibers produced via the oil−water system, the proposed all-in-water microfluidic system would expand the range of use of hydrogel fibers such as the encapsulation of hydrophilic substances in the aqueous droplets, which was first reported in this work. Furthermore, this method would be beneficial for well tailoring the hydrogel fiber containing a series of aqueous droplets, which could serve as a cell-friendly carrier for controllably encapsulating components with a specific content.

Since we introduced pneumatic valves to facilitate the generation of ADHF containing aqueous droplets, the effects of valve switch cycle on D_d, D_t, and D_f were also studied systematically. As a result, the valve switch cycle (0.2−0.5 s) could influence not only D_d (increased from 48.71 ± 6.13 to 99.19 ± 5.61 μm, Figure 2N) but also D_t (significantly increased 3.85-fold from 0.2 to 0.5 s, Figure 2O), whereas the valve switch cycle had no significant influence on D_f (Figure 2P). As shown in Figure 2N, the droplets generated with the aid of pneumatic valves (0.4 s) exhibited uniform features and a smaller coefficient of variation (CV = 6.92%). So, a larger diameter and distance of aqueous droplets can be easily fabricated by increasing the valve switch cycle in the device. The higher droplet generation frequency results in the denser packing modes for the encapsulation of aqueous droplets in the fiber. In our system, we easily change the loading capacity of aqueous droplets in fibers by adjusting relative parameters (flow rates and valve cycle, Figure 2), demonstrating that ADHF could serve as a potential implantable substance delivery carrier to meet different needs of chemical and biological applications.

The function and application of the ADHF containing aqueous droplets largely depended on the ADHF morphology that was affected by the flow rates and valve switch cycle of the all-in-water system. To explore the effects of the valve switch cycle on the fiber morphological characterization, a fluorescent

https://dx.doi.org/10.1021/acsami.0c20434
ACS Appl. Mater. Interfaces XXXX, XXX, XXX−XXX

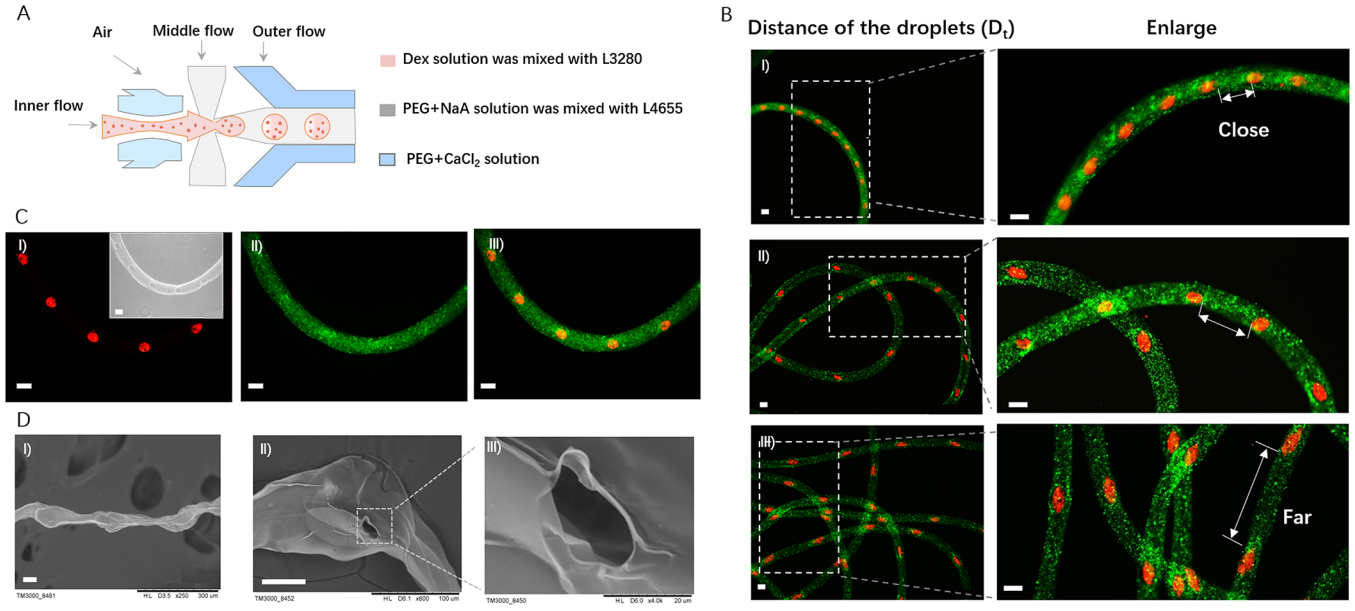

Figure 3. Characterization of the morphology and structure of ADHF. (A) Schematic diagram of the forming of the fibers with aqueous droplets. Droplet = red, fiber = green: the Dex solution and PEG solution that contained NaA were added with red and green fluorescent polystyrene nanoparticles, respectively. (B) Fluorescence images of ADHF under varying valve switch cycles from 0.3, 0.5, to 0.6 s. The inner-phase, middle-phase, and the outer-flow rates were fixed to 0.1, 2, and 40 μL/min, respectively. Scale bars: 100 μm. (C) Fluorescence images and the bright-field image of ADHF on the certain condition to show the details of droplets and fiber (valve cycle: 0.4 s, and the inner-phase, middle-phase, and the outer-flow rates were 0.1, 2, and 40 μL/min, respectively). Scale bars: 100 μm. (D) (I) Overall SEM images of freeze-dried ADHF. (II, III) Characterization of the hollow cavity structure of the ADHF (valve cycle: 0.3 s, and the inner-phase, middle-phase, and the outer-flow rates were 0.1, 2, and 40 μL/min, respectively). Scale bars: 50 μm.

microscope and scanning electron microscope (SEM) were used to characterize the ADHF.

The fluorescent microscope was an expedient equipment to intuitively observe the morphology of transparent materials. A schematic diagram of ADHF formation via the all-in-water microfluidic system is shown in Figure 3A. To visualize the structure of ADHF, we added L4655 (green) and L3280 (red) fluorescent polystyrene nanoparticles in the inner phase and middle phase, respectively (Figure 3A). Here, we chose the valve switch cycles to visualize the distance of the droplets in ADHF. The results show that the fibers generated in this work were entire and continuous. The distance of droplets could be easily operated and separated in a controllable way, and corresponding change of D_t can be performed (172.67 ± 27.43 to 468.85 ± 37.25 μm, Figure 3B). To vividly illustrate the well-defined spatial distribution, we showed the droplets' and fibers' location, respectively (Figure 3C). A distinct partition of droplets and fibers was observed without cross-contamination between them. During the generation of the ADHF, NaA in the middle phase could not diffuse into the inner phase (Figure S3). These results revealed that the ADHF could be beneficial to the co-encapsulation of the diverse components in a controllable spatial arrangement, which could meet many potential requirements and exhibit multiple useful properties with flexible functionalities.

To reveal the droplet-filled structure in the fibers, the ADHFs were treated in the lyophilizer for freeze drying in situ, and then they were characterized by using SEM (Figure 3D). As shown in Figure 3D(I), the ADHF was intact, smooth, and continuous, demonstrating that our method could effectively reduce the risk of spheroid loss, which supplied more feasibility to the transplant process. In addition, the ADFH apparently shrinks at the area of intervals between templated droplets and exhibits spindle-knotted architecture. The images of a freeze-dried ADHF exhibited the hollow cavity structure in the fibers (as shown in Figure 3D(II,III), which was induced by the diffusion of Dex from the fiber into the water. The fiber structure with a series of aqueous cavities was difficult to obtain in the traditional way. These results also demonstrated the high hydration property of the ADHF materials, which is one of the key properties for biological applications.

To verify the feasibility, operability, and biocompatibility of ADHF as 3D carriers for tissue engineering application, we cultured the islet organoids in the aqueous droplets of fibers with one-step operation. Before the generation of islet organoids, hiPSCs are induced and differentiated into endoderm, pancreatic endoderm, and endocrine progenitor cells sequentially in a six-well plate according to previous reports.[43,44] Then, the pancreatic endocrine progenitor cells are resuspended in the inner phase (Dex solution, 1×10^7 cells mL^{-1}) and encapsulated into aqueous droplets within CaA fibers (Figure 1C). The endocrine progenitor cells are self-organized into islet organoids after encapsulation in fibers at day 1 (Figure 4A). Moreover, these organoids could further differentiate in 7 days, demonstrating the feasibility of generation and culture of the organoids in ADHF with the all-aqueous microfluidic system. We qualitatively analyze the cell viability of organoids using live/dead assay. The results demonstrate that the viability of the organoids is good in the fibers for at least 7 days (Figure 4A). The live cell ratio in the organoids is stable and higher than 80% through 1 week (Figure 4B), demonstrating the great biocompatibility of the materials and the mild condition of the spinning process. To further examine the cell viability of islets organoids, the caspase 3 marker indicated that apoptotic cells were immunostained and quantified (Figure S4). The results show that about 2% of

https://dx.doi.org/10.1021/acsami.0c20434
ACS Appl. Mater. Interfaces XXXX, XXX, XXX−XXX

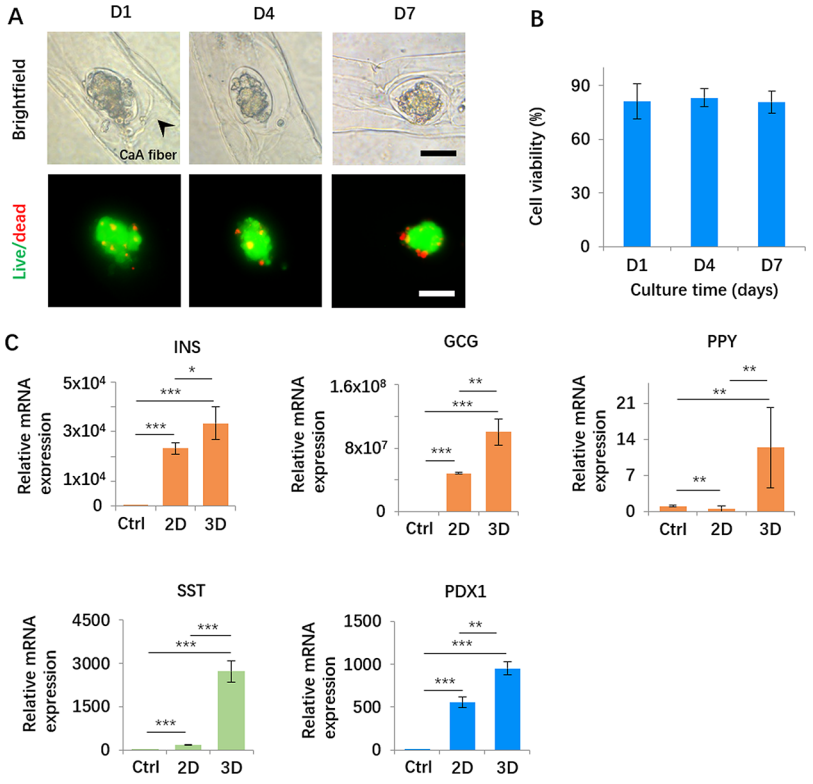

Figure 4. Encapsulation and generation of hiPSC-derived islet organoids in ADHF. (A) Representative bright-field images and fluorescent images of the ADHF after encapsulating pancreatic endocrine progenitor cells for 1, 4, and 7 days. The green and red fluorescence represent live and dead cells, respectively (valve cycle: 0.4 s; the inner-phase, middle-phase, and the outer-flow rates were 0.1, 2, and 40 μL/min, respectively). (B) Cell viability of islet organoids is detected at days 1, 4, and 7 in ADHF based on the fluorescence quantitative analysis. (C) Comparison of the pancreatic maturity-related gene expression in the undifferentiated hiPSC (Ctrl), differentiated cells cultured in a 2D plate (2D) for 7 days, and differentiated organoids in 3D fibers for 7 days (3D); the results were tested by PCR. The expression values are normalized to the GAPDH. *p < 0.05, **p < 0.01, and ***p < 0.001. Scale bars: 50 μm.

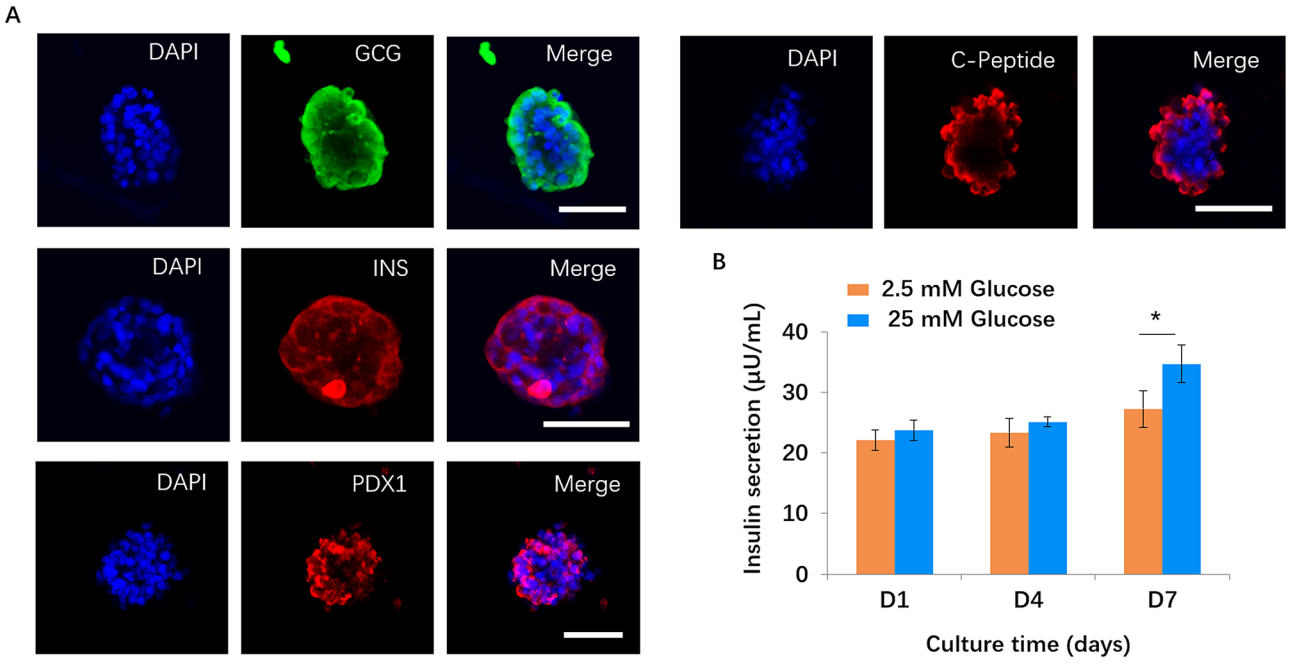

Figure 5. Biofunctions of islet organoids encapsulated in ADHF. (A) Immunofluorescent images of pancreatic endocrine hormone markers INS, GCG, PPY, and PDX1 in islet organoids at 7 days of culture. (B) Insulin secretion of islet organoids exposed to 2.5 and 25 mM glucose for 30 min of incubation within the fibers. About 100 organoids were measured in each group using ELISA. *p < 0.05. Scale bars: 50 μm.

the cells were apoptotic cells in islet organoids, exhibiting favorable cell activity. Also, the proliferation ability of the encapsulated islet organoids was tested using a CCK-8 assay kit during the culture period (Figure S4). To double evaluate the

https://dx.doi.org/10.1021/acsami.0c20434
ACS Appl. Mater. Interfaces XXXX, XXX, XXX−XXX

cellular growth vitality, we measured the size of islet organoids at days 1 and 7. The islet organoids maintained an average diameter of 60−65 μm after 1 and 7 days of culture in ADHF. These data suggest that organoids can keep their size and not proliferate basically. The results are consistent with our previous report.[43] Furthermore, the throughput to generate the pancreatic progenitor cell-loaded droplets was 150 droplets/min (pneumatic valves 0.4 s), which was much higher than the traditional well-plate method (about several cellular organoids/min).[45] The throughput could be further increased by upregulating the cycle of pneumatic valves. The mean diameter of the islet organoids was 60.66 ± 4.71 μm (coefficient of variation, CV = 7.77%) after 7 days of culture, which exhibited the uniformity of organoid formation in ADFH than in the well plate.[46,47] Especially, as shown in Figure 4A, the diameter of islet organoids was limited by the dimension of the droplet, which means that the size of organoids could be flexibly controlled via tuning the D_d within the ADHF. The islet organoid-laden fibers were continuous and intact, which did not degrade for the culture of 7 days, showing the good stability of the ADHF during the culture period (Figure 4A and Figure S4d). These results suggest that all aqueous environment is highly mild and suitable for cell 3D culture, self-assembly, and organoid formation in ADHF. For the first time, we realize the formation and differentiation of stem cell organoids in ADHF in a groundbreaking way.

To further verify the biocompatibility and potential of the ADHF as 3D scaffolds, we culture the islet organoids in 2D plates and 3D fibers for 7 days. Then, the differentiation and maturation of islet organoids[44] were assessed by using the real-time PCR (Figure 4C). The results showed that the expressions of insulin secretion-associated marker insulin (INS), α-cell marker glucagon (GCG), pancreatic polypeptide (PPY), β cell-associated pancreatic duodenal homeobox 1 (PDX1), and somatostatin (SST) were very low in the undifferentiated hiPSCs. After 7 days of differentiation, the expressions of the above markers were upregulated in a 2D plate, which exhibited the feasibility of our differentiation protocols. As to the organoids in 3D fibers, the expression of the above islet-related genes further increased remarkably compared to that in the 2D culture. These results indicate the presence of pancreatic β cells and α cells in islet organoids, proving the importance of ADHF on the differentiation and maturity of islet organoids under more physiological micro-environments.

To double check the differentiation of the islet organoids within ADHF, hormone-related markers (INS, GCG, PPY, and PDX1) were evaluated in islet organoids on day 7 as well (Figure 5A). The immunofluorescent results exhibited significant expression of hormone proteins in organoids, which further reveal the maturity and bio-functionality of islet organoids. As widely known, a vital functional trait of the islets (β-cells) is the ability to implement GSIS.[44] We tested the insulin secretion of about 100 islet organoids within the ADHF in response to the treatments of low/high-glucose at days 1, 4, and 7, respectively (Figure 5B). The results show that the islet organoids could maintain insulin secretion up to at least 7 days. In addition, there was a significant increase in the insulin secretion in islet organoids with high glucose treatment (25 mM) at 7 days. These results indicated that the generated islet organoids within ADHF displayed the function of insulin secretion, and the islet organoids were more mature after 7 days of differentiation, which showed a sensitive response to high-glucose stimulation.

Compared to previously reported methods,[48,49] our approach avoids a multi-step and tedious process in fabrication of cell spheroid-laden fibers. Furthermore, it has feasibility and operability to generate organoid-laden ADHF, which were formed in a flexible and convenient way. As above, the human islet organoids generated within ADHF display good viability and excellent islet-related functions, which prove that the ADHF is a suitable scaffold for the 3D culture of organoids with flexible operability and great biocompatibility. Also, the ADHF could reduce the hypoxia in large implantable scaffolds.[50] These results demonstrated that our platform could generate stable and uniform organoids with controllable distances and sizes within fibers, which were useful for modeling the construction of organoids in vitro. In addition, we have partially addressed the existing challenge in DHF fabrication with an oil-free system. Without the encapsulated oil−water interface,[36,38] the molecular diffusion and nutrient exchange in the fibers are obviously increased. Owing to the unique structures and proper biocompatibility of ADFH scaffolds, our method may provide an alternative way to translational therapy of diabetes by simultaneously loading growth factors and proteins with stem cells or organoids, which could be readily implanted into the human body.

CONCLUSIONS

In this work, we presented a novel all-in-water microfluidic system for one-step generation of aqueous-droplet-filled hydrogel fiber with flexible properties and configurations. By integrating the pneumatic valve, the generation of ADHF could be facilitated with the improved controllability and the enhanced operability. Stable aqueous droplets are created based on the separation of active phases of the dextran and polyethylene glycol as well as the fast cross-linking of the sodium alginate and calcium chloride in the droplet-laden fibers. The ADHF produced in this work are entire, continuous, and repeatable. The size and the distance of the droplets within the ADHF can be flexibly controlled by tuning the flow rates and the valve switch cycle. The uniformly arranged droplets in this fiber could increase the capability of the fibers and reduce the hypoxia in large implantable scaffolds. The ADHF with separated droplets can be beneficial to the co-encapsulation of the diverse components without cross-contamination in a controllable spatial arrangement. Furthermore, we prove that the ADHF fabricated in this work is a suitable scaffold for organoid generation. The hiPSC-derived islet organoids are formed in our ADHF, which exhibit good cell viability and maintain islet-related functions. The proposed all-in-water microfluidic system holds promise for fabrication of multifunctional scaffolds with good biocompatibility and permeability, which could be used to carry various cells, micro-tissues, and bio-factors.

EXPERIMENTAL SECTION

Materials. Dex (Mw = 500 kDa) and PEG (Mw = 20 kDa) were purchased from Sigma. NaA (55 cps) was bought from Qingdao Hyzlin Biology Development Co., Ltd. Anhydrous $CaCl_2$ and NaCl were purchased from Tianjin Damao Chemical Reagents Factory. Red (L3280) and green (L4655) fluorescent polystyrene nanoparticles with average sizes of ∼0.5 and ∼1 μm, respectively, were purchased from Sigma-Aldrich. FITC-NaA (R-F8801) was purchased from Ruixibio.

https://dx.doi.org/10.1021/acsami.0c20434
ACS Appl. Mater. Interfaces XXXX, XXX, XXX−XXX

Microfluidic Chip Manufacture. The polydimethylsiloxane (PDMS) microfluidic chip was processed via conventional lithography as follows.[51] The chip is composed of two pieces of PDMS layers. The top layer with microchannels was templated from an SU-8 (Microchem, USA) mold and then was bonded to a blank PDMS layer undergoing oxygen plasma cleaning. The height of the channel is 200 μm. The widths of the inner, middle, and outer flow channels and the gas channel are 100, 350, 200, and 200 μm, respectively. The width of inner flow channel located between the pneumatic valves is 50 μm, and the width between the inner flow channel and valve's chamber is 45 μm.

ADHF Generation and Characterization. According to the existing reports,[36,40] Dex and PEG were chosen in the all-in-water system due to good biocompatibility. The following reagents were injected into the microfluidic chip: (1) a Dex (15% (w/w)) solution was injected into the inner flow channel, (2) a mixed solution that contained PEG (17% (w/w)) and NaA (1% (w/w)) was injected into the middle flow channel, (3) a mixed solution that contained PEG (17% (w/w)) and $CaCl_2$ (4% (w/w)) was introduced into the outer flow channel. A PEG (17% (w/w)) solution in a bath was used to collect the ADHF. All solutions were dissolved in deionized water. According to our previous report,[51] 17 wt % PEG (Mw = 20 kDa) and 15 wt % Dex (Mw = 500 kDa) can be served as optimum concentrations to generate stable and uniform droplets. The ADHF was characterized using an optical microscope (Leica), fluorescence microscope (Olymplus), scanning microscope (TM3000), and imageJ. We first determined the direction of the ellipse based on the longest axis of the ellipse in order to measure the major axis and the minor axis of the elliptic droplets in ADHF. Then, we chose the longest axis of the ellipse as the longitudinal diameter of droplets and a perpendicular bisector to the longest axis as the horizontal diameter for each ellipse. Thus, we used the average value of vertical and horizontal diameters to calculate D_d. To further characterize the structure of ADHF, we mixed the FITC-NaA (green, final concentration: 1 mg/mL) in the middle flow.

Human iPSC Culture and Induction. The hiPSCs were offered by Prof. Ning Sun (Fudan University). HiPSCs were cultured on Matrigel (diluted, 1:50)-coated six-well plates (Guangzhou Jet Bio-Filtration Co., Ltd.) with an mTeSR1 medium (Stem Cell) in a cell incubator and induced to generate pancreatic endocrine cells by a sequential medium in different stages as follows. First, hiPSCs were induced to definitive endoderm (DE) cells in a medium including DMEM/F12 (Invitrogen, 94% (v/v)), activin-A (PeproTech, 100 ng mL^{-1}), KSR (Invitrogen, 1% (v/v)), GlutaMAX (Invitrogen, 1% (v/v)), B27 (Invitrogen, 1% (v/v)), and penicillin−streptomycin (Sigma, 1% (v/v)) for 5 days. Then, DE cells were differentiated to pancreatic endoderm (PE) cells in a medium containing DMEM (Invitrogen, 95.5% (v/v)), B27 (0.5% (v/v)), dorsomorphin (Selleck, 2 μM), retinoic acid (Sigma, 2 μM), SB431542 (Selleck, 10 μM), basic fibroblast growth factor (R&D systems, 5 ng mL^{-1}), and SANT-1 (Selleck, 250 nM) for 6 days. Next, PE cells were induced to endocrine progenitor (EP) cells under the medium containing DMEM (95.5% (v/v)), B27 (0.5% (v/v), dorsomorphin (2 μM), SB431542 (10 μM), ascorbic acid (Sigma, 50 μg mL^{-1}), and DAPT (Abcam Biochemicals, 10 μM) for 4 days. After that, the medium was changed with CMRL 1066 (Invitrogen) containing glucose (Sigma, 25 mM), B27 (0.5% (v/v), nicotinamide (Sigma, 10 mM), SB431542 (10 μM), ascorbic acid (Sigma, 50 μg mL^{-1}), and dorsomorphin (2 μM) for a subsequent culture.

Cells Encapsulation. Pancreatic endocrine cells were digested using accutase and trypsin−EDTA (Gibco) at 1:1 volume ratio and resuspended in inner flow (density, 1×10^7 cells mL^{-1}). CMRL 1066 medium containing resuspended cells was mixed with 22.5% (w/w) Dex and 0.9% (w/w) NaCl in a 1:2 volume ratio as inner flow. The solution containing 17% (w/w) PEG, 1% (w/w) NaA and 0.9% (w/w) NaCl was served as middle flow. 17% (w/w) PEG and 4% (w/w) $CaCl_2$ was used as outer flow. 17% (w/w) PEG and 0.9% (w/w) NaCl was filled in a collection bath. ADHF generated were collected using a rotary spool. The gelled ADHF with cells were rapidly shifted to a culture plate, in which the medium was replaced by fresh culture solution every day. We chose 0.9% (w/w) NaCl added to the inner flow, the middle flow and the collection bath to maintain the physiological osmotic pressure and to avoid the damage of cells during the experimental operation.

Cell Viability. The cell viability in ADHF was detected at 1, 4, and 7 days of culture. The live and dead cells were stained either green or red color with a conventional live/dead kit (BD) as previous reports.[52] The viability of organoids was calculated through dividing the area of green fluorescence to the total area of green and red fluorescence.

CCK-8 Assay. The assay of the cellular growth vitality was quantified at 1, 4, and 7 days of culture using a CCK-8 kit (Dojindo, CK04) as previous reports.[51]

Insulin Assay. The insulin secretion response of islet organoids in ADHF was measured using a kit (Jiangsu Biological Technology Co., Ltd.). Cell-laden ADHFs were put into a culture plate and soaked in Krebs−Ringer buffer (KRB) solution for 2 h. Then, the samples were exposed to KRB solutions containing 2.5 and 25 mM glucose for 0.5 h. Fresh KRB solution containing 2.5 mM glucose was used to rinse samples three times in each step. Finally, the supernatants were collected and detected using an ELISA kit (ATECE Diagnostics).

Real-Time Quantitative PCR. The sample was treated as with a previous protocol.[53] Real-time quantitative PCR was operated via an SYBR Green kit (TAKARA) under 40 cycles. The relative primer pairs are shown in the Supporting Information, Table 1. We unified the concentrations of the mRNA (600 ng/mL), which were consistent in the control, 2D, and 3D groups (10^6 cells/group). Quantification was performed using GAPDH as the internal reference gene.

Fluorescence Immunohistochemistry. ADHF-encapsulated islet organoids were collected after 7 days of culture. The sample was treated following the previous steps.[54] The relative primary antibodies, secondary antibodies, and cell nuclei staining reagents are listed in the Supporting Information, Table 2. Here, we co-stained DAPI and caspase 3 in the samples. The area ratio of the caspase 3 and DAPI was counted as the percentages of the caspase 3 positive cells.

Statistics. Experiments were performed at least three times. All data are shown as mean ± standard deviation. Statistical significance was defined as $*p$ value <0.05, $**p < 0.01$, and $***p < 0.001$ by a one-way analysis of variance and Student's t-test.

■ ASSOCIATED CONTENT

Supporting Information

The Supporting Information is available free of charge at https://pubs.acs.org/doi/10.1021/acsami.0c20434.

Bright-field images of the generation of ADHF in the absence of the pneumatic valve; statistical distribution of the droplets under various conditions; confocal laser scanning microscopy images of the ADHF; examination of cell viability and proliferation ability in islet organoids at days 1, 4 and 7; list of primer pairs for real-time quantitative PCR; and list of primary antibodies, secondary antibodies, and cell nuclei staining reagents used for immunostaining (PDF)

■ AUTHOR INFORMATION

Corresponding Author

Jianhua Qin − *Division of Biotechnology, CAS Key Laboratory of SSAC, Dalian Institute of Chemical Physics, Chinese Academy of Sciences, Dalian 116023, China; Institute For Stem Cell and Regeneration, Chinese Academy of Sciences, Beijing 100101, China; CAS Center for Excellence in Brain Science and Intelligence Technology, Chinese Academy of Sciences, Shanghai 200031, China; University of Chinese Academy of Sciences, Beijing 100049, China;* orcid.org/0000-0001-5735-6436; Email: jhqin@dicp.ac.cn

https://dx.doi.org/10.1021/acsami.0c20434
ACS Appl. Mater. Interfaces XXXX, XXX, XXX−XXX

Authors

Hui Wang − *Division of Biotechnology, CAS Key Laboratory of SSAC, Dalian Institute of Chemical Physics, Chinese Academy of Sciences, Dalian 116023, China; University of Chinese Academy of Sciences, Beijing 100049, China*

Haitao Liu − *Division of Biotechnology, CAS Key Laboratory of SSAC, Dalian Institute of Chemical Physics, Chinese Academy of Sciences, Dalian 116023, China; University of Chinese Academy of Sciences, Beijing 100049, China*

Xu Zhang − *Department of Biomedical Engineering, Duke University, Durham, North Carolina 27708, Unites States*

Yaqing Wang − *Division of Biotechnology, CAS Key Laboratory of SSAC, Dalian Institute of Chemical Physics, Chinese Academy of Sciences, Dalian 116023, China; University of Chinese Academy of Sciences, Beijing 100049, China*

Mengqian Zhao − *Division of Biotechnology, CAS Key Laboratory of SSAC, Dalian Institute of Chemical Physics, Chinese Academy of Sciences, Dalian 116023, China; University of Chinese Academy of Sciences, Beijing 100049, China*

Wenwen Chen − *Division of Biotechnology, CAS Key Laboratory of SSAC, Dalian Institute of Chemical Physics, Chinese Academy of Sciences, Dalian 116023, China; University of Chinese Academy of Sciences, Beijing 100049, China*

Complete contact information is available at: https://pubs.acs.org/10.1021/acsami.0c20434

Author Contributions

[&]H.W., H.L., and X.Z. contributed equally to this work.

Notes

The authors declare no competing financial interest.

■ ACKNOWLEDGMENTS

This research was supported by the Strategic Priority Research Program of the Chinese Academy of Sciences (nos. XDA16020900, XDB32030200, and XDB29050301), National Science and Technology Major Project (no. 2018ZX09201017-001-001), National Nature Science Foundation of China (nos. 31971373, 81703470), and Innovation Program of Science and Research from the DICP, CAS (DICP I201934).

■ REFERENCES

(1) Zhang, Y.; Ding, J.; Qi, B.; Tao, W.; Wang, J.; Zhao, C.; Peng, H.; Shi, J. Multifunctional Fibers to Shape Future Biomedical Devices. *Adv. Funct. Mater.* **2019**, *29*, 1902834.

(2) Du, X. Y.; Li, Q.; Wu, G.; Chen, S. Multifunctional Micro/Nanoscale Fibers Based on Microfluidic Spinning Technology. *Adv. Mater.* **2019**, *31*, 1903733.

(3) Chen, W.; Guo, Z. Hierarchical Fibers for Water Collection Inspired by Spider Silk. *Nanoscale* **2019**, *11*, 15448−15463.

(4) Cao, K.; Shen, L.; Guo, X.; Wang, K.; Hu, X.; Ouyang, X.; Zhao, G. Hydrogel Microfiber Encapsulation Enhances Cryopreservation of Human Red Blood Cells with Low Concentrations of Glycerol. *Biopreserv. Biobanking* **2020**, *18*, 228−234.

(5) Gao, Y.; Jin, X. Dual Crosslinked Methacrylated Alginate Hydrogel Micron Fibers and Tissue Constructs for Cell Biology. *Mar Drugs.* **2019**, *17*, 557.

(6) Liu, H.; Wang, Y.; Cui, K.; Guo, Y.; Zhang, X.; Qin, J. Advances in Hydrogels in Organoids and Organs-on-a-Chip. *Adv. Mater.* **2019**, *31*, 1902042.

(7) Pedde, R. D.; Mirani, B.; Navaei, A.; Styan, T.; Wong, S.; Mehrali, M.; Thakur, A.; Mohtaram, N. K.; Bayati, A.; Dolatshahi-Pirouz, A.; Nikkhah, M.; Willerth, S. M.; Akbari, M. Emerging Biofabrication Strategies for Engineering Complex Tissue Constructs. *Adv. Mater.* **2017**, *29*, 1606061.

(8) Chen, C.; Tang, J.; Gu, Y.; Liu, L.; Liu, X.; Deng, L.; Martins, C.; Sarmento, B.; Cui, W.; Chen, L. Bioinspired Hydrogel Electrospun Fibers for Spinal Cord Regeneration. *Adv. Funct. Mater.* **2019**, *29*, 1806899.

(9) An, D.; Chiu, A.; Flanders, J. A.; Song, W.; Shou, D.; Lu, Y. C.; Grunnet, L. G.; Winkel, L.; Ingvorsen, C.; Christophersen, N. S.; Fels, J. J.; Sand, F. W.; Ji, Y.; Qi, L.; Pardo, Y.; Luo, D.; Silberstein, M.; Fan, J.; Ma, M. Designing a Retrievable and Scalable Cell Encapsulation Device for Potential Treatment of Type 1 Diabetes. *Proc. Natl. Acad. Sci. U. S. A.* **2018**, *115*, E263−E272.

(10) Talebian, S.; Shim, I. K.; Kim, S. C.; Spinks, G. M.; Vine, K. L.; Foroughi, J. Coaxial Mussel-Inspired Biofibers: Making of a Robust and Efficacious Depot for Cancer Drug Delivery. *J. Mater. Chem. B* **2020**, *8*, 5064−5079.

(11) Ju, M.; Wu, B.; Sun, S.; Wu, P. Redox-Active Iron-Citrate Complex Regulated Robust Coating-Free Hydrogel Microfiber Net with High Environmental Tolerance and Sensitivity. *Adv. Funct. Mater.* **2020**, *30*, 1910387.

(12) Wei, S.; Qu, G.; Luo, G.; Huang, Y.; Zhang, H.; Zhou, X.; Wang, L.; Liu, Z.; Kong, T. Scalable and Automated Fabrication of Conductive Tough-Hydrogel Microfibers with Ultrastretchability, 3D Printability, and Stress Sensitivity. *ACS Appl. Mater. Interfaces* **2018**, *10*, 11204−11212.

(13) Sim, H. J.; Jang, Y.; Kim, H.; Choi, J. G.; Park, J. W.; Lee, D. Y.; Kim, S. J. Self-Helical Fiber for Glucose-Responsive Artificial Muscle. *ACS Appl. Mater. Interfaces* **2020**, *12*, 20228−20233.

(14) Lee, H. J.; Koh, W. G. Hydrogel Micropattern-Incorporated Fibrous Scaffolds Capable of Sequential Growth Factor Delivery for Enhanced Osteogenesis of hMSCs. *ACS Appl. Mater. Interfaces* **2014**, *6*, 9338−9348.

(15) Johnson, C. D. L.; Ganguly, D.; Zuidema, J. M.; Cardinal, T. J.; Ziemba, A. M.; Kearns, K. R.; McCarthy, S. M.; Thompson, D. M.; Ramanath, G.; Borca-Tasciuc, D. A.; Dutz, S.; Gilbert, R. J. Injectable, Magnetically Orienting Electrospun Fiber Conduits for Neuron Guidance. *ACS Appl. Mater. Interfaces* **2019**, *11*, 356−372.

(16) Mirani, B.; Pagan, E.; Shojaei, S.; Dabiri, S. M. H.; Savoji, H.; Mehrali, M.; Sam, M.; Alsaif, J.; Bhiladvala, R. B.; Dolatshahi-Pirouz, A.; Radisic, M.; Akbari, M. Facile Method for Fabrication of Meter-Long Multifunctional Hydrogel Fibers with Controllable Biophysical and Biochemical Features. *ACS Appl. Mater. Interfaces* **2020**, *12*, 9080−9089.

(17) Kong, B.; Chen, Y.; Liu, R.; Liu, X.; Liu, C.; Shao, Z.; Xiong, L.; Liu, X.; Sun, W.; Mi, S. Fiber Reinforced GelMA Hydrogel to Induce the Regeneration of Corneal Stroma. *Nat. Commun.* **2020**, *11*, 1435.

(18) Luo, G.; Yu, Y.; Yuan, Y.; Chen, X.; Liu, Z.; Kong, T. Freeform, Reconfigurable Embedded Printing of All-Aqueous 3D Architectures. *Adv. Mater.* **2019**, *31*, 1904631.

(19) Guo, J.; Yu, Y.; Wang, H.; Zhang, H.; Zhang, X.; Zhao, Y. Conductive Polymer Hydrogel Microfibers from Multiflow Microfluidics. *Small* **2019**, *15*, e1805162.

(20) Yu, Y.; Wei, W.; Wang, Y.; Xu, C.; Guo, Y.; Qin, J. Simple Spinning of Heterogeneous Hollow Microfibers on Chip. *Adv. Mater.* **2016**, *28*, 6649−6655.

(21) Yamada, M.; Seki, M. Multiphase Microfluidic Processes to Produce Alginate-Based Microparticles and Fibers. *J. Chem. Eng. Jpn.* **2018**, *51*, 318−330.

(22) Wang, G.; Jia, L.; Han, F.; Wang, J.; Yu, L.; Yu, Y.; Turnbull, G.; Guo, M.; Shu, W.; Li, B. Microfluidics-Based Fabrication of Cell-Laden Hydrogel Microfibers for Potential Applications in Tissue Engineering. *Molecules* **2019**, *24*, 1633.

(23) Onoe, H.; Okitsu, T.; Itou, A.; Kato-Negishi, M.; Gojo, R.; Kiriya, D.; Sato, K.; Miura, S.; Iwanaga, S.; Kuribayashi-Shigetomi, K.; Matsunaga, Y. T.; Shimoyama, Y.; Takeuchi, S. Metre-long cell-laden

microfibres exhibit tissue morphologies and functions. *Nat. Mater.* **2013**, *12*, 584−590.
(24) Shi, X.; Ostrovidov, S.; Zhao, Y.; Liang, X.; Kasuya, M.; Kurihara, K.; Nakajima, K.; Bae, H.; Wu, H.; Khademhosseini, A. Microfluidic Spinning of Cell-Responsive Grooved Microfibers. *Adv. Funct. Mater.* **2015**, *25*, 2250−2259.
(25) Kang, E.; Choi, Y. Y.; Chae, S. K.; Moon, J. H.; Chang, J. Y.; Lee, S. H. Microfluidic Spinning of Flat Alginate Fibers with Grooves for Cell-Aligning Scaffolds. *Adv. Mater.* **2012**, *24*, 4271−4277.
(26) Jia, L.; Han, F.; Yang, H.; Turnbull, G.; Wang, J.; Clarke, J.; Shu, W.; Guo, M.; Li, B. Microfluidic Fabrication of Biomimetic Helical Hydrogel Microfibers for Blood-Vessel-on-a-Chip Applications. *Adv. Healthcare Mater.* **2019**, *8*, 1900435.
(27) Shao, L.; Gao, Q.; Zhao, H.; Xie, C.; Fu, J.; Liu, Z.; Xiang, M.; He, Y. Fiber-Based Mini Tissue with Morphology-Controllable GelMA Microfibers. *Small* **2018**, *14*, 1802187.
(28) Yu, Y.; Fu, F.; Shang, L.; Cheng, Y.; Gu, Z.; Zhao, Y. Bioinspired Helical Microfibers from Microfluidics. *Adv. Mater.* **2017**, *29*, 1605765.
(29) Sun, T.; Hu, C.; Nakajima, M.; Takeuchi, M.; Seki, M.; Yue, T.; Shi, Q.; Fukuda, T.; Huang, Q. On-Chip Fabrication and Magnetic Force Estimation of Peapod-Like Hybrid Microfibers Using a Microfluidic Device. *Microfluid. Nanofluid.* **2014**, *18*, 1177−1187.
(30) Deng, X.; Ren, Y.; Hou, L.; Liu, W.; Jiang, T.; Jiang, H. Compound-Droplet-Pairs-Filled Hydrogel Microfiber for Electric-Field-Induced Selective Release. *Small* **2019**, *15*, 1903098.
(31) Deng, X.; Ren, Y.; Hou, L.; Liu, W.; Jia, Y.; Jiang, H. Electric Field-Induced Cutting of Hydrogel Microfibers with Precise Length Control for Micromotors and Building Blocks. *ACS Appl. Mater. Interfaces* **2018**, *10*, 40228−40237.
(32) Chaurasia, A. S.; Jahanzad, F.; Sajjadi, S. Flexible Microfluidic Fabrication of Oil-Encapsulated Alginate Microfibers. *Chem. Eng. J.* **2017**, *308*, 1090−1097.
(33) Wang, W.; He, X. H.; Zhang, M. J.; Tang, M. J.; Xie, R.; Ju, X. J.; Liu, Z.; Chu, L. Y. Controllable Microfluidic Fabrication of Microstructured Materials from Nonspherical Particles to Helices. *Macromol. Rapid Commun.* **2017**, *38*, 1700429.
(34) Chaurasia, A. S.; Sajjadi, S. Flexible Asymmetric Encapsulation for Dehydration-Responsive Hybrid Microfibers. *Small* **2016**, *12*, 4146−4155.
(35) Yu, Y.; Wen, H.; Ma, J.; Lykkemark, S.; Xu, H.; Qin, J. Flexible Fabrication of Biomimetic Bamboo-Like Hybrid Microfibers. *Adv. Mater.* **2014**, *26*, 2494−2499.
(36) Zhu, K.; Yu, Y.; Cheng, Y.; Tian, C.; Zhao, G.; Zhao, Y. All-Aqueous-Phase Microfluidics for Cell Encapsulation. *ACS Appl. Mater. Interfaces* **2019**, *11*, 4826−4832.
(37) Xie, R.; Xu, P.; Liu, Y.; Li, L.; Luo, G.; Ding, M.; Liang, Q. Necklace-Like Microfibers with Variable Knots and Perfusable Channels Fabricated by an Oil-Free Microfluidic Spinning Process. *Adv. Mater.* **2018**, *30*, 1705082.
(38) Liu, C.; Zheng, W.; Xie, R.; Liu, Y.; Liang, Z.; Luo, G.; Ding, M.; Liang, Q. Microfluidic Fabrication of Water-in-Water Droplets Encapsulated in Hydrogel Microfibers. *Chin. Chem. Lett.* **2019**, *30*, 457−460.
(39) Chao, Y.; Shum, H. C. Emerging Aqueous Two-Phase Systems: from Fundamentals of Interfaces to Biomedical Applications. *Chem. Soc. Rev.* **2020**, *49*, 114−142.
(40) Ma, Q.; Song, Y.; Sun, W.; Cao, J.; Yuan, H.; Wang, X.; Sun, Y.; Shum, H. C. Cell-Inspired All-Aqueous Microfluidics: From Intracellular Liquid-Liquid Phase Separation toward Advanced Biomaterials. *Adv. Sci.* **2020**, *7*, 1903359.
(41) Jeyhani, M.; Thevakumaran, R.; Abbasi, N.; Hwang, D. K.; Tsai, S. S. H. Microfluidic Generation of All-Aqueous Double and Triple Emulsions. *Small* **2020**, *16*, 1906565.
(42) Agarwal, P.; Zhao, S.; Bielecki, P.; Rao, W.; Choi, J. K.; Zhao, Y.; Yu, J.; Zhang, W.; He, X. One-Step Microfluidic Generation of Pre-hatching Embryo-Like Core-Shell Microcapsules for Miniaturized 3D Culture of Pluripotent Stem Cells. *Lab Chip* **2013**, *13*, 4525−4533.
(43) Liu, H.; Wang, Y.; Wang, H.; Zhao, M.; Tao, T.; Zhang, X.; Qin, J. A Droplet Microfluidic System to Fabricate Hybrid Capsules Enabling Stem Cell Organoid Engineering. *Adv. Sci.* **2020**, *7*, 1903739.
(44) Tao, T.; Wang, Y.; Chen, W.; Li, Z.; Su, W.; Guo, Y.; Deng, P.; Qin, J. Engineering Human Islet Organoids from iPSCs Using an Organ-on-Chip Platform. *Lab Chip* **2019**, *19*, 948−958.
(45) Candiello, J.; Grandhi, T. S. P.; Goh, S. K.; Vaidya, V.; Lemmon-Kishi, M.; Eliato, K. R.; Ros, R.; Kumta, P. N.; Rege, K.; Banerjee, I. 3D Heterogeneous Islet Organoid Generation from Human Embryonic Stem Cells Using a Novel Engineered Hydrogel Platform. *Biomaterials* **2018**, *177*, 27−39.
(46) Tang, Y.; Zuniga-Hertz, J. P.; Han, C.; Yu, B.; Cai, D. Multifaceted Secretion of htNSC-Derived Hypothalamic Islets Induces Survival and Antidiabetic Effect via Peripheral Implantation in Mice. *Elife* **2020**, *9*, e52580.
(47) Brboric, A.; Vasylovska, S.; Saarimäki-Vire, J.; Espes, D.; Caballero-Corbalan, J.; Larfors, G.; Otonkoski, T.; Lau, J. Characterization of Neural Crest-Derived Stem Cells Isolated from Human Bone Marrow for Improvement of Transplanted Islet Function. *Ups. J. Med. Sci.* **2019**, *124*, 228−237.
(48) Nguyen, T. P. T.; Le, N. X. T.; Lee, N. Y. Microfluidic Approach to Generate a Tadpole-Egg-Shaped Alginate Fiber and Its Application in Tissue Engineering. *ACS Biomater. Sci. Eng.* **2020**, *6*, 1663−1670.
(49) Jun, Y.; Kang, A. R.; Lee, J. S.; Jeong, G. S.; Ju, J.; Lee, D. Y.; Lee, S. H. 3D Co-culturing Model of Primary Pancreatic Islets and Hepatocytes in Hybrid Spheroid to Overcome Pancreatic Cell Shortage. *Biomaterials* **2013**, *34*, 3784−3794.
(50) Desai, T.; Shea, L. D. Advances in Islet Encapsulation Technologies. *Nat. Rev. Drug Discov.* **2017**, *16*, 338−350.
(51) Liu, H. T.; Wang, H.; Wei, W. B.; Liu, H.; Jiang, L.; Qin, J. H. A Microfluidic Strategy for Controllable Generation of Water-in-Water Droplets as Biocompatible Microcarriers. *Small* **2018**, *14*, 1801095.
(52) Wang, H.; Liu, H.; He, F.; Chen, W.; Zhang, X.; Zhao, M.; Wang, L.; Qin, J. Flexible Generation of Multi-Aqueous Core Hydrogel Capsules Using Microfluidic Aqueous Two-Phase System. *Adv. Mater. Technol.* **2020**, *5*, 2000045.
(53) Wang, Y.; Wang, H.; Deng, P.; Chen, W.; Guo, Y.; Tao, T.; Qin, J. In situ Differentiation and Generation of Functional Liver Organoids from Human iPSCs in a 3D Perfusable Chip System. *Lab Chip* **2018**, *18*, 3606−3616.
(54) Wang, H.; Liu, H.; Liu, H.; Su, W.; Chen, W.; Qin, J. One-Step Generation of Core−Shell Gelatin Methacrylate (GelMA) Microgels Using a Droplet Microfluidic System. *Adv. Mater. Technol.* **2019**, *4*, 1800632.

https://dx.doi.org/10.1021/acsami.0c20434
ACS Appl. Mater. Interfaces XXXX, XXX, XXX−XXX